NEOPLASIA
www.neoplasia.com

Volume 11 Number 9 September 2009 pp. 910–920 910

Dynamic Contrast-Enhanced Magnetic Resonance Imaging of Vascular Changes Induced by Sunitinib in Papillary Renal Cell Carcinoma Xenograft Tumors[1]

Gilda G. Hillman*, Vinita Singh-Gupta*, Hao Zhang*, Areen K. Al-Bashir†,‡, Yashwanth Katkuri†,‡, Meng Li†,‡, Christopher K. Yunker*, Amit D. Patel*, Judith Abrams§ and E. Mark Haacke†,‡

*Department of Radiation Oncology, Barbara Ann Karmanos Cancer Institute, Wayne State University School of Medicine, Detroit, MI 48201, USA; †Department of Radiology, Barbara Ann Karmanos Cancer Institute, Wayne State University School of Medicine, Detroit, MI 48201, USA; ‡Department of Biomedical Engineering, Barbara Ann Karmanos Cancer Institute, Wayne State University School of Medicine, Detroit, MI 48201, USA; §Integrated Biostatistics Unit, Barbara Ann Karmanos Cancer Institute, Wayne State University School of Medicine, Detroit, MI 48201, USA

Abstract

To investigate further the antiangiogenic potential of sunitinib for renal cell carcinoma (RCC) treatment, its effects on tumor vasculature were monitored by dynamic contrast-enhanced magnetic resonance imaging (DCE-MRI) using an orthotopic KCI-18 model of human RCC xenografts in nude mice. Tumor-bearing mice were treated with various doses of sunitinib, and vascular changes were assessed by DCE-MRI and histologic studies. Sunitinib induced dose-dependent vascular changes, which were observed both in kidney tumors and in normal kidneys by DCE-MRI. A dosage of 10 mg/kg per day caused mild changes in Gd uptake and clearance kinetics in kidney tumors. A dosage of 40 mg/kg per day induced increased vascular tumor permeability with Gd retention, probably resulting from the destruction of tumor vasculature, and also caused vascular alterations of normal vessels. However, sunitinib at 20 mg/kg per day caused increased tumor perfusion and decreased vascular permeability associated with thinning and regularization of tumor vessels while mildly affecting normal vessels as confirmed by histologic diagnosis. Alterations in tumor vasculature resulted in a significant inhibition of KCI-18 RCC tumor growth at sunitinib dosages of 20 and 40 mg/kg per day. Sunitinib also exerted a direct cytotoxic effect in KCI-18 cells *in vitro*. KCI-18 cells and tumors expressed vascular endothelial growth factor receptor 2 and platelet-derived growth factor receptor β molecular targets of sunitinib that were modulated by the drug treatment. These data suggest that a sunitinib dosage of 20 mg/kg per day, which inhibits RCC tumor growth and regularizes tumor vessels with milder effects on normal vessels, could be used to improve blood flow for combination with chemotherapy. These studies emphasize the clinical potential of DCE-MRI in selecting the dose and schedule of antiangiogenic compounds.

Neoplasia (2009) 11, 910–920

Abbreviations: RCC, renal cell carcinoma; DCE-MRI, dynamic contrast-enhanced magnetic resonance imaging; ROI, region of interest; IAUC, initial area under the curve; CIAUC, cumulative IAUC; VEGFR-2, vascular endothelial growth factor receptor 2; VEGF, vascular endothelial growth factor; PDGFR-β, platelet-derived growth factor receptor β; KCI-18 RCC, Karmanos Cancer Institute-18 RCC cell line; KCI-18/IK, KCI-18 RCC cell line passaged in mouse kidney; RTK, receptor tyrosine kinase; PFS, progression-free survival; Gd-DTPA, gadolinium diethylene triamine pentaacetic acid; SU10, sunitinib 10 mg/kg per day; SU20, sunitinib 20 mg/kg per day; SU40, sunitinib 40 mg/kg per day; H&E, hematoxylin-eosin; NK, normal kidney; KT, kidney tumor

Address all correspondence to: Gilda G. Hillman, PhD, Department of Radiation Oncology, 515 Hudson-Webber Cancer Research Center, 4100 John R. Road, Detroit, MI 48201.
E-mail: hillmang@karmanos.org

[1]This study was supported by Pfizer grant IIR no. GA61818Z 9 (to G.G. Hillman).
Received 14 April 2009; Revised 5 June 2009; Accepted 6 June 2009

DOI 10.1593/neo.09618

Introduction

Renal cell carcinoma (RCC) incidence has increased in recent years with approximately 54,390 new cases each year in the United States. The disease is responsible for an estimated 13,010 deaths each year [1]. Nearly half of the patients present with localized disease that can be treated by surgical removal [2,3]. However, one third of the patients have metastatic disease at first presentation, and 20% to 30% of the patients treated for localized RCC subsequently develop metastatic disease that frequently involves the lungs [2,3]. The median survival of patients with metastatic RCC ranged from 8 to 11 months [2–4]. The treatment of metastatic RCC remains a significant challenge, but recent developments in antiangiogenic therapy have improved targeting these highly vascularized tumors.

The vascular endothelial growth factor (VEGF), produced by tumor cells and associated stromal cells, is a key growth factor in the angiogenic process, which promotes the proliferation, migration, and invasion of endothelial cells and plays a role in vascular permeability [5]. Targeting the tumor vasculature with antiangiogenic therapy has been shown to suppress the growth of established tumors in mice, leading to several clinical trials with different angiogenesis inhibitors [5,6]. Numerous antiangiogenic compounds recently developed include anti-VEGF antibodies and inhibitors of receptor tyrosine kinases (RTKs). The drug sunitinib (SU11248 or Sutent) is a small-molecule RTK inhibitor that has demonstrated antitumor and antiangiogenic activities in mouse xenograft models. Sunitinib targets and inhibits signaling of several RTKs including platelet-derived growth factor receptor (PDGFR), VEGF receptor (VEGFR), c-kit protooncogene, and FMS-like tyrosine kinase 3 [7–13]. Sunitinib exhibits direct antitumor activity by inhibiting RTKs that are expressed by cancer cells and are involved in signaling for cancer cell proliferation [7]. Sunitinib also exhibits antiangiogenic activity by inhibition of signaling through VEGFR-2 and PDGFR-β RTKs expressed on endothelial cells or stromal cells [7]. Initial clinical trials with sunitinib for metastatic RCC showed significant responses in multiple metastatic sites and in primary tumors resulting in 40% partial response rate with a median time to progression of 8.7 months [14]. These studies justified approval of sunitinib by the FDA in January 2006 for RCC treatment. In a phase 3 multinational study of 750 patients with metastatic RCC, randomized to sunitinib or interferon α, the response rate to sunitinib was 31%, with median progression-free survival (PFS) of 11.7 months and a median survival of 28 months [15]. A recent update of this trial documented an objective response rate of 47% with 11 months of median PFS for sunitinib *versus* 12% objective response rate and 5 months of PFS for interferon α [16]. Although the results with sunitinib therapy are impressive, long-term control of the disease is still not achieved. In addition, several trials documented adverse effects of cardiotoxicity in some of the patients, probably as a result of alterations to normal vasculature [17–20]. Therefore, further investigations with sunitinib dose adjustments are warranted to decrease the impact on vital organs such as the heart and the kidney.

The goal of our study was to investigate the effect of lower and potentially less toxic doses of sunitinib on tumor vasculature to establish the conditions for combination therapies to determine whether a combined strategy could maintain and improve efficacy. Disruption of the tumor vasculature to deprive tumor cells from nutrients by sunitinib, given in conjunction with cytotoxic therapies, could be more effective in preventing progression of metastatic RCC. However, this approach could be a paradox given that complete destruction of tumor vasculature could compromise the efficacy of chemotherapy or radiotherapy because both depend on blood flow to the tumor for delivering oxygen and drugs [21,22]. To improve the blood flow in tumors, the concept of "normalization" of tumor vasculature is based on the regularization of tumor vessels by pruning or destroying immature and inefficient blood vessels through elimination of excess endothelial cells, and it has shown promise for combination therapies [23–27]. The process of tumor angiogenesis involves proliferation of abnormal vessels that are enlarged, disorganized, and leaky due to the defective basement membrane. These structural defects of tumor vessels cause increased interstitial tissue pressure, impaired blood supply, and decreased oxygen supply in tumors compromising the delivery and efficacy of cytotoxic drugs and radiotherapy [21,22]. The challenge is to develop imaging technologies that monitor early vascular changes and induction of tumor vasculature normalization by antiangiogenic drugs for scheduling cytotoxic therapy.

We selected to use dynamic contrast-enhanced magnetic resonance imaging (DCE-MRI) to investigate the effect of sunitinib therapy on RCC tumor vasculature using a preclinical papillary RCC murine model. DCE-MRI is a noninvasive approach, currently used in humans, that can detect early changes in the tumor induced by antiangiogenic therapy as reported in human studies [28–31] and in preclinical animal models [32,33]. This method measures a combination of tumor perfusion and vessel permeability and allows the detection of changes in tumor vascularity, which occur at a much earlier stage in the treatment of tumors with antiangiogenic drugs than does shrinkage of tumor mass [29,31]. Contrast agents typically consist of gadolinium (Gd)-based chelates with paramagnetic properties that are used to enhance signal from the tissue in clinical MRI. The contrast agent, injected intravenously, enters the extravascular extracellular space through the capillary bed as a function of perfusion and permeability. The contrast agent that accumulates over time in the tumor can be then analyzed by MRI [29,31]. Recent animal studies suggest that parametric images providing information on the morphology and function of the microvasculature of tumors can be obtained by Gd-DTPA–based DCE-MRI [34].

DCE-MRI was performed using an orthotopic RCC model in athymic nude mice, which was established by subcapsular renal implantation of Karmanos Cancer Institute-18 (KCI-18) cells, a tumor cell line generated from a human papillary RCC specimen in our laboratory [35]. Vascular changes induced by various doses of sunitinib in tumor-bearing kidneys and normal contralateral kidneys were monitored by DCE-MRI and by histologic studies of tissue sections.

Materials and Methods

Orthotopic KCI-18/IK RCC Tumor Model

The human RCC cell line designated KCI-18 was established in our laboratory from a primary renal tumor specimen obtained from a patient with papillary RCC (nuclear grade 3/4) [35]. Cells were cultured in Dulbecco's modified Eagle medium with supplements [35]. After serial passages of KCI-18 cells in the kidney of nude mice, highly tumorigenic KCI-18/IK were generated [35]. KCI-18/IK cells were washed with Hank's balanced salt solution and subcapsularly injected at a concentration of 5×10^5 cells in 30 μl of Hank's balanced salt solution in the right kidney in 5- to 6-week-old female BALB/C *nu/nu* nude mice (Harlan, Indianapolis, IN) [35]. Mice were housed and handled under sterile conditions in facilities accredited by the American Association for the Accreditation of Laboratory Animal Care. The animal protocol was approved by the Animal Investigation Committee of Wayne State University.

Experimental Protocol

After injection of KCI-18/IK cells, a few mice were killed at early time points to assess tumor growth before initiating treatment. Small tumors were detectable by days 9 to 10 in the kidney. By days 10 to 12, mice bearing established kidney tumors (KTs) were treated with sunitinib (Pfizer, Inc, New York, NY). The drug was prepared in a carboxymethyl cellulose suspension vehicle, at dosages of 10, 20, or 40 mg/kg per day (SU10, SU20, or SU40, respectively) and given orally by gavage, once a day [7]. Control mice were treated with vehicle only. Treatment was continued for 7 to 18 days. On the basis of initial experiments, early time points of 7-day sunitinib treatment were selected for DCE-MRI studies or for monitoring RTKs expression to avoid incorrect analysis of advanced and large necrotic tumors in control mice. For DCE-MRI experiments, three mice per treatment group were imaged. To assess the therapeutic response of KTs to an optimal dosage of 40 mg/kg per day of sunitinib, 10 mice per experimental group were treated daily for 18 days. For sunitinib dose-response studies, eight mice per experimental group were treated daily with 10, 20 or 40 mg/kg per day of sunitinib. Mice were killed by day 28 after tumor cell injection, when the tumor burden in control animals was large (>1.5 cm × 1 cm in size compared with 0.7 cm × 0.25 cm for normal kidney [NK]) to compare with tumor sizes in treated groups. Tumor-bearing kidneys were resected and weighed [35].

Tissue Preparation for Histologic Diagnosis

At completion of experiments, mice were killed and KTs as well as the contralateral NKs were resected and processed for histologic diagnosis. All tissues were fixed in 10% buffered formalin, embedded in paraffin, and sectioned [35]. Sections were stained with hematoxylin-eosin (H&E) [35]. Tissue sections were also immunostained with anti-CD31 antibody (Ab; Thermo Scientific, Fremont, CA) using an avidin-biotin immunoperoxidase technique [35].

DCE-MRI Monitoring of Tumor Perfusion and Permeability and Tumor Size in KTs

Mice from control and sunitinib-treated groups were imaged by DCE-MRI. Mice were anesthetized by intraperitoneal injections of 0.35 ml of pentobarbital and 0.35 ml of ketamine at a concentration of 52.5 mg/kg then a catheter was inserted into their tail vein, which was attached to a syringe containing Gd-DTPA contrast agent (Berlex, Wayne, NJ). Mice were positioned on a cradle heated by temperature-controlled water and were given a second low dose of anesthetics of 15 mg/kg each in 0.1 ml to avoid motion problems while in the magnet. A 2-cm-diameter receive-only surface coil was placed over the tumor, and the cradle was placed inside an 11-cm inner-diameter transmit-only volume coil. DCE-MRI of mice was performed in the MR Research Facility at Wayne State University using a Bruker Biospec AVANCE animal scanner (Bruker, Karlsruhe, Germany) equipped with a 4.7-T horizontal bore magnet and actively shielded gradients. Anatomic imaging was done using a two-dimensional T2-weighted spin-echo scan (repetition time = 2000 milliseconds, echo time = 52.4 milliseconds) to get an overview of the kidney. Baseline imaging data of the kidneys were obtained using the short-repetition time DCE scan for 30 time points (7 seconds between time points). On time point 10, 100 μl of Gd-DTPA (0.125 mmol/kg) was injected into the tail vein catheter. This dose was selected based on preliminary Gd dose-searching experiments to obtain appropriate contrast for image analysis. Then, imaging data were acquired for 20 more time points. The imaging parameters for this multislice two-dimensional gradient echo scan were as follows: repetition time = 54.7 milliseconds, echo time = 2.9 milliseconds, flip angle = 30 degrees, field of view = 32 mm × 32 mm, slice thickness = 1.5 mm with 0.5-mm gap, matrix size = 128 × 128. Five slices were collected for each animal. Data were processed to determine changes in contrast agent uptake using the SPIN DCE software (Detroit, MI) [36]. For data analysis, the full kidney was selected as the region of interest (ROI) for the KT and the contralateral left NK. A threshold was selected to remove noise-only pixels in the image. Gd concentrations [$C(t)$] in the tissue were calculated for all pixels in the ROI and for each time point [36]. Data from the $C(t)$ curves were compiled for each pixel for 16 time points (112 seconds) after Gd injection to create the initial area under the curve (IAUC). The distribution of IAUC for the entire ROI is then shown as a means to visualize the effects in every pixel in a single plot. The CIAUC is the cumulative initial area under the curve of the IAUC histogram. For quantitative analysis of vascular permeability, R50 (median) values are derived from CIAUC curves and correspond to the concentration of Gd at which 50% of the pixels have been included [36]. To evaluate the kinetics of uptake, washout, and leakage into the kidney tissue and tumor, the parametric color maps are used to show the initial rate of uptake, peak concentration and clearance of Gd in the tissue, and individual structures in each slice. The parameters measured in DCE-MRI for sunitinib-treated tumors were compared with those obtained for control tumors and NKs.

Analysis of Cell Survival by Clonogenic Assay

KCI-18 cells were treated with sunitinib doses of 0.1 to 5 μM and plated in a colony formation assay, in triplicate wells of six-well plates at 500 cells per well for control and 0.1 μM sunitinib, at 1000 cells per well for 0.5 and 1 μM sunitinib, and at 3000 cells per well for 2.5 and 5 μM sunitinib [37]. After 10 days of incubation at 37°C in a 5% CO_2/5% O_2/90% N_2 incubator, colonies were counted, the plating efficiency was calculated for each well, and the surviving fraction was normalized to control cells [37].

Expression of VEGFR-2 and PDGFR-β on KCI-18 Cells and KCI-18 KTs

KCI-18 RCC cells, cultured in flasks, were harvested and processed for lysis and protein extraction [37]. To detect the expression of VEGFR-2 and PDGFR-β, cell protein extracts were first immunoprecipitated, overnight at 4°C, with specific Abs directed against VEGFR-2 (Santa Cruz Biotechnology, Inc, Santa Cruz, CA) and PDGFR-β (Millipore, Temecula, CA). Immune complexes were separated using protein A agarose beads (Millipore) [7,9], and receptor expressions were determined by Western blot analysis using 8% SDS-PAGE gels. KTs were snap-frozen in liquid N_2. Tumors (100 mg) were lysed for protein extraction using HNTG lysis buffer containing protease inhibitors before Western blot analysis [7,9].

Statistical Analysis

Evaluation of the shape of the frequency distribution of tumor weights indicated that a log transformation was required to meet the assumptions of normal theory tests. Two-sample *t*-tests were used to assess the significance of differences in tumor weight between mice treated with SU40 and control mice. A linear model with indicator variables to parameterize dose was used to investigate the relationship of vehicle, SU dose, and tumor weight. The paired difference in weight between the NK and KT was calculated and compared between experimental groups. Adjustment for multiple comparisons between treatments was

made using Holm's [38] procedure to protect against inflated type I errors [37].

Results

DCE-MRI of KTs

To investigate the effect of sunitinib on tumor vasculature, mice-bearing KTs were imaged by MRI before and after contrast Gd injection. We report the data of a representative experiment comparing three dosages of sunitinib, namely, 10, 20, and 40 mg/kg per day, to control mice treated with vehicle. These sunitinib dosages were selected based on previous animal studies demonstrating that 40 mg/kg per day of sunitinib, given daily, is a biologically active dosage [7].

For data analysis, the full kidney was selected as the ROI both for the right KT and the left NK (Figure 1*A*, T1). Gd concentrations [C(t)] were calculated for all pixels in each ROI and for each time point, and the average C(t) over all pixels was plotted (Figure 1*B*) [36]. C(t) values, obtained after Gd injection, were integrated during 16 time points (112 seconds) to create the $IAUC_{112}$ histograms (Figure 1*C*) and CIAUC (Figure 1*D*). In control mice, Gd uptake was rapid in both the KT and NK. However, the kinetics of clearance of Gd in the KT were slow compared with faster clearance in the NK (C(t) in Figure 1*B*). Indeed, the IAUC/CIAUC curves for the KT showed a pronounced shift to the right compared with NK, indicative of a greater retention of Gd (Figure 1, *C* and *D*). DCE-MRI of mice treated with SU40 revealed a pattern of Gd uptake that remained at a

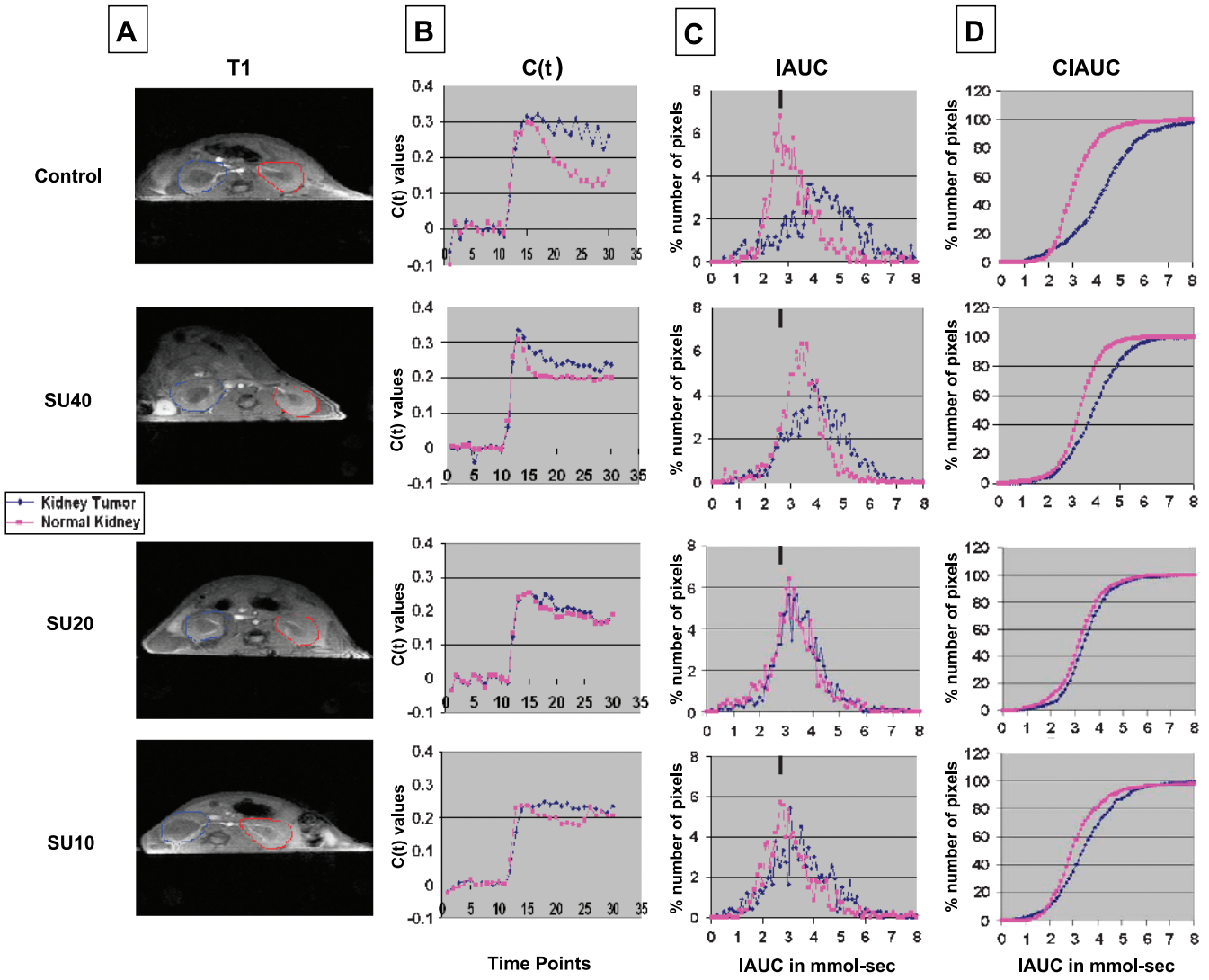

Figure 1. DCE-MRI of KCI-18 KTs. Mice bearing established tumors in the right kidneys were treated every day for 7 days with vehicle only (control) or with sunitinib at dosages of 40, 20, or 10 mg/kg per day (SU40, SU20, or SU10, respectively). Then, mice were imaged by DCE-MRI for 30 time points at 7-second intervals. (A) Baseline images were collected for the first during 10 time points before Gd contrast agent injection. At time point 10, Gd was injected in the tail vein, and images were collected for 20 more time points. For data analysis, the full kidney was selected as the ROI for the KT (blue contour on left of T1 image) and the contralateral left NK (red contour on right of T1 image). A threshold was selected to remove noise only pixels in the image. (B) The kinetics of Gd contrast uptake are represented in C(t) curves. (C) Data from the C(t) curves were compiled for 16 time points (112 seconds) after Gd injection to draw $IAUC_{112}$. The small black bar indicates the peak position of NK in control mice and can be used as a reference for curve shifting in NKs and KTs treated with sunitinib. (D) The CIAUC graphs were derived from IAUC curves. In panels B, C, and D, blue lines are for KTs and pink lines are for NKs. Data from a representative mouse from each treatment group are presented.

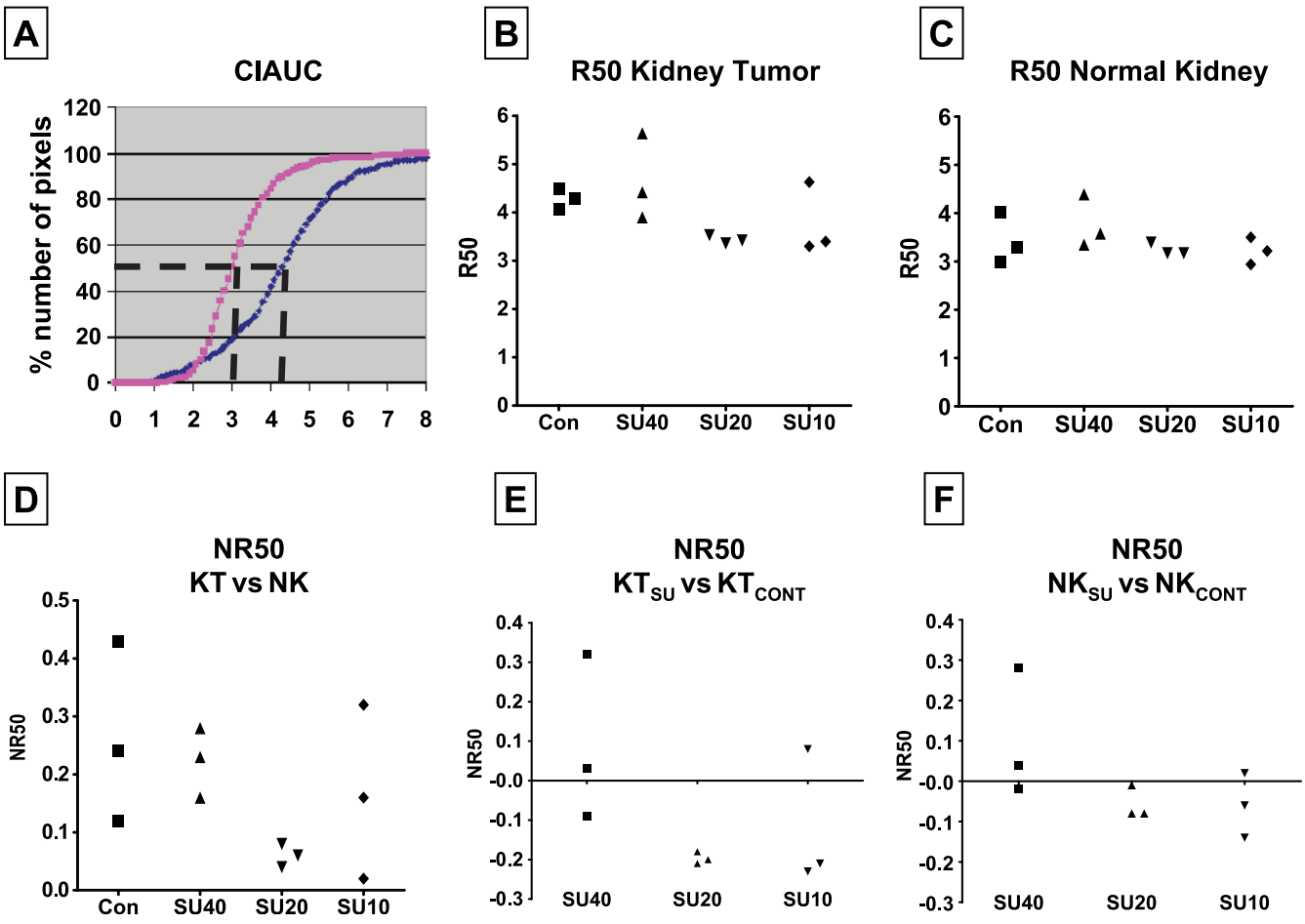

Figure 2. R50 quantitation of DCE-MRI data of KCI-18 KTs. (A) The R50 value is derived from CIAUC curves (as shown for control mouse) and corresponds to the Gd concentration at which 50% of the pixels have been included. (B) R50 of KTs from three mice per treatment group. (C) R50 of contralateral NK from the same three mice per treatment group shown in panel B. (D) NR50 of KT *versus* NK: NR50 represents normalization of R50 values of KTs relative to R50 values of contralateral NK calculated as [$R50_{KT}$ − $R50_{NK}$] / $R50_{NK}$ for each mouse and shown for three mice per group. (E) NR50 of KT_{SU} *versus* KT_{CONT}: Normalization of R50 values of KTs from mice treated with sunitinib (KT_{SU}) relative to the mean R50 values of KTs from control mice (KT_{CONT}) calculated as [R50 KT_{SU} − R50 $KT_{mean\ cont}$] / R50 $KT_{mean\ cont}$ for each mouse and shown for three mice per treatment group. (F) NR50 of NK_{SU} *versus* NK_{CONT}: Normalization of R50 values of NKs of mice treated with sunitinib relative to the mean R50 values of NKs from control mice calculated as [R50 NK_{SU} − R50 $NK_{mean\ cont}$] / R50 $NK_{mean\ cont}$ for each mouse and shown for three mice per treatment group. Data are presented for three mice per treatment group from the same experiment shown in Figure 1.

plateau with more retention of Gd in both kidneys compared with control mice. Retention of Gd was still greater in the KT treated with sunitinib than in the NK as observed by a shift to the right in IAUC/CIAUC curves relative to NK, but this shift was less pronounced than in control tumors (Figure 1, *C* and *D*). In mice treated with SU20, patterns of Gd uptake and clearance were identical in the KT and the NK (Figure 1*B*). SU20 mice had IAUC and CIAUC overlapping with those of the NK, indicative of improved tumor perfusion (Figure 1, *C* and *D*). Interestingly, the KT IAUC curve looked more regular and shifted to the left compared with KTs in control or SU40-treated mice, indicating decreased Gd retention. SU10 also seemed to change the kinetics of uptake and clearance in KTs, showing a shift to the left in IAUC curves compared with control or SU40-treated mice but less than with SU20-treated tumors (Figure 1, *C* and *D*). In the NK, SU10 caused milder changes in Gd uptake and clearance than SU20 or SU40 and resulted in an IAUC pattern comparable to that of NK in control mice (Figure 1, *C* and *D*). It should be noted that compared with tumors from control mice, sunitinib treatment at all tested dosages caused significant shifts to the left of IAUC curves of KTs, which were more pronounced with lower SU20 and SU10 doses than with a higher SU40 dose (as visualized relative to the *black bar on top of each graph* in Figure 1*C*). Vascular changes in NKs were observed with higher SU20 and SU40 dosages and were expressed by a shift to the right in IAUC curves compared with NKs of control mice. These data presented for one mouse per treatment group were consistently observed for two additional mice per group in the same experiment showing reproducibility of our findings.

To compare the patterns of Gd uptake in KTs *versus* NKs, R50 values for three mice per treatment group were derived from CIAUC curves for both KTs and NKs (Figure 2). The R50 (median) values correspond to the concentration of Gd at which 50% of the pixels have been included (Figure 2*A*) [36]. A trend in lower R50 values was observed in SU10- and SU20-treated mice compared with control mice and SU40-treated mice for both R50 of KTs (Figure 2*B*) and NKs (Figure 2*C*). R50 values of KTs were then normalized to the R50 values of contralateral NKs for each mouse and shown as normalized R50 values (NR50) for three mice per group (Figure 2*D*) [36]. We found

that NR50 of KTs relative to NKs were consistently much smaller in SU20-treated mice in a range of 0.04 to 0.08 compared with a wide range of 0.12 to 0.43 in SU10-treated, SU40-treated, or control mice (Figure 2*D*). When NR50 was calculated as R50 values of KTs from sunitinib-treated mice relative to KTs from control mice, NR50 of SU20-treated mice was consistently lower than that of SU40-treated mice (Figure 2*E*). A trend to lower NR50 values was also observed with SU10-treated mice (Figure 2*E*). To assess the effect of sunitinib on contralateral NKs, R50 values of NKs from mice treated with sunitinib were normalized to NKs from control mice (Figure 2*F*). These NR50 data of NKs showed lower values for SU10- and SU20-treated mice compared with SU40-treated mice (Figure 2*F*).

DCE-MRI Analysis of Gd Kinetics of Uptake and Clearance Using Parametric Color Maps

The parametric color maps from control mice showed accumulation of Gd in the periphery of the tumor with no uptake in the core of the tumor (Figure 3). In the NK of control mice, Gd uptake was distributed in the entire kidney with a higher uptake in the medullary central area than in the peripheral cortex, probably reflecting normal secretion of contrast agent (Figure 3). The negative slope image (Nslope) represents the clearance kinetics of Gd and shows low levels in control mice. The kidneys of SU40-treated mice showed a strong accumulation of Gd in most of the KT with persisting high levels in the peak, slope, and washout slope images (Figure 3). This effect was also observed in the NK with increased levels of Gd in both cortex and medulla, indicating that this high dosage of sunitinib also alters the perfusion of NK tissue. Parametric color maps of SU20-treated mice showed a significant accumulation of Gd in the KT including Gd uptake in the tumor (Figure 3). These levels were high in the peak, slope, and Nslope images. Similar findings were observed in NK treated with SU20 (Figure 3). In contrast, KTs from SU10-treated mice showed no uptake of Gd in the core of the tumor, but some was seen at its periphery similar to KTs from control mice (Figure 3). Low levels were observed in the peak, slope, and Nslope images. The NK of mice treated with SU10 showed more Gd in the medulla than in the cortex (Figure 3) as seen in NK of control mice. These findings were consistently observed in two additional mice per group.

Therapeutic Response of KTs to Sunitinib

Previous studies using sunitinib in mouse tumor models have demonstrated that dosages of 40 or 80 mg/kg per day were optimal and biologically active, leading to tumor inhibition and inhibition of phosphorylation of RTKs on cancer cells and endothelial cells [7–9]. Therefore, for our initial studies, we selected to test an optimal dosage of 40 mg/kg per day of sunitinib to investigate the therapeutic response of KTs using our KCI-18 RCC model. After intrarenal injection of KCI-18 cells, by days 10 to 12, mice developed established KTs

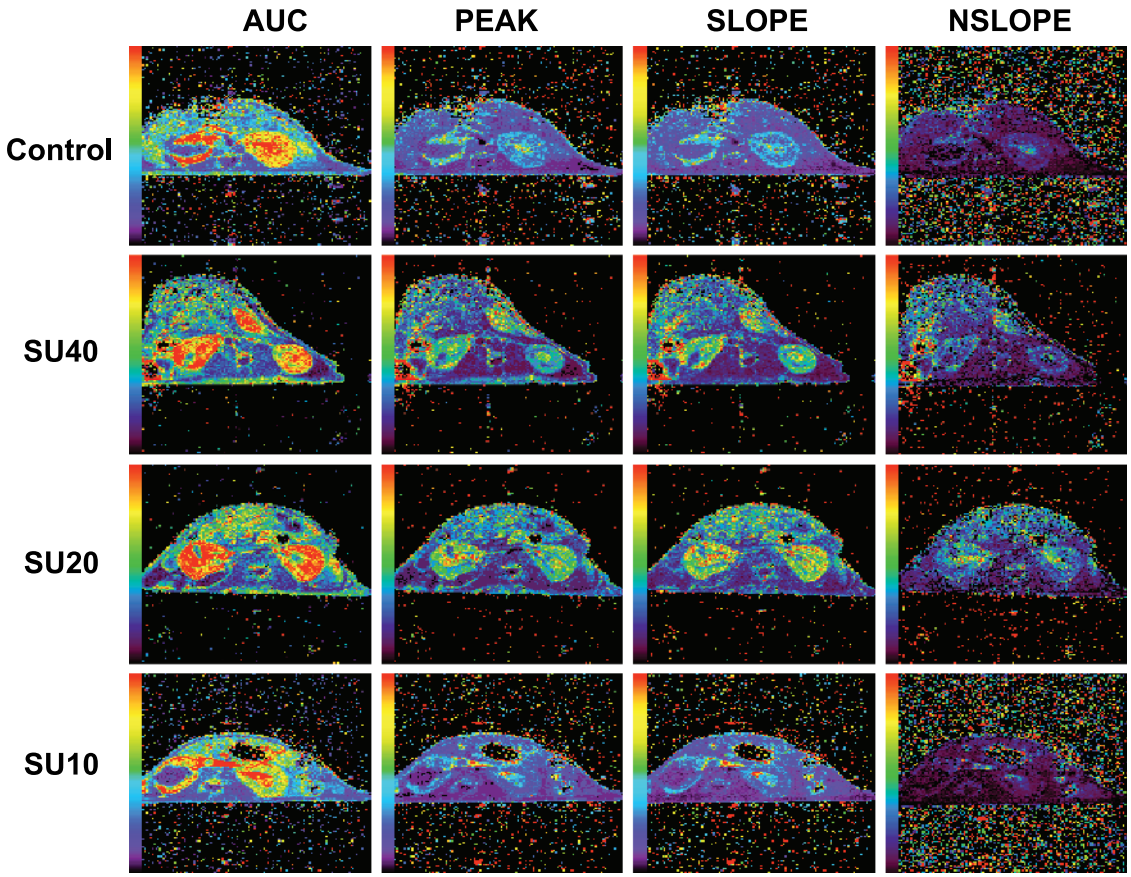

Figure 3. DCE-MRI of KTs: Parametric color maps. Parametric color maps were constructed based on uptake and concentration of Gd in the tissue, represented by the colors blue, green, yellow, and red with gradual increase of Gd from lowest values (blue) to highest values (red). Data are presented for the same representative mouse from each treatment group shown in Figure 1. The KT is on the left, and the contralateral NK is on the right of the MR images. The color coding in the kidneys are shown for IAUC, the peak, and the slope of $C(t)$. The Nslope represents the clearance of Gd after reaching the peak in the tissue.

with a mean (SD) volume of 150 (7) mm^3 and mean (SD) weight of 186 (4) mg compared with NK volume of 125 (2) mm^3 and weight of 148 (12) mg. At that time point, mice were treated daily with 40 mg/kg per day of sunitinib. On day 28 after cell injection, the right KT and the left NK were weighed (Figure 4*A*). On average, KTs in control animals were 822 mg heavier than the contralateral NK. After sunitinib treatment, KTs were significantly smaller compared with control mice (P = .0001; Figure 4*A*). On average, SU40-treated tumors were 75% smaller than tumors in control mice but were still significantly larger compared with the contralateral NKs, with a mean (SD) difference of 209 (105) mg (P < .0001; Figure 4*A*, *inset*). The weight disparity between the tumor-bearing and the NK was significantly smaller in mice treated with SU40 compared with control animals (P = .0002). By gross observation, control mice showed very large and extremely vascularized tumors that invaded the entire kidney and grew into the abdominal cavity (Figure 4*A*, *inset*). After sunitinib treatment, the shape of the kidney was preserved in KTs indicating that SU40 therapy controlled the growth and invasion of the tumor through kidney tissue, but the kidneys looked ischemic.

DCE-MRI findings suggest that lower doses of sunitinib have a different effect on tumor perfusion; therefore, in additional separate experiments, a dose-response study of sunitinib was tested, and a representative experiment is presented in Figure 4*B*. The therapeutic efficacy of lower dosages of 10 or 20 mg/kg per day of sunitinib was evaluated and compared with that of 40 mg/kg per day. SU10 did not significantly control KT growth (P = .43); tumors were only 25% smaller than control tumors on average (Figure 4*B*) and appeared more hemorrhagic by gross observation. Both SU20 and SU40 significantly inhibited KT growth; average growth inhibition was 57% and 66%, respectively, relative to control tumors (P = .003 and P = .0007, respectively; Figure 4*B*). On average, tumors of SU20-treated mice were 43% smaller than tumors of SU10-treated mice, but the difference is only marginally significant (P = .05). Although the tumors of SU40-treated mice were not significantly smaller than those of SU20-treated mice (P = .55), the variation in tumor size from mouse to mouse was smaller in SU40-treated mice (Figure 4*B*). The extent of tumor growth inhibition mediated by SU40 was comparable in these two series of independent experiments presented in Figure 4, *A* and *B*, confirming reproducibility of our findings.

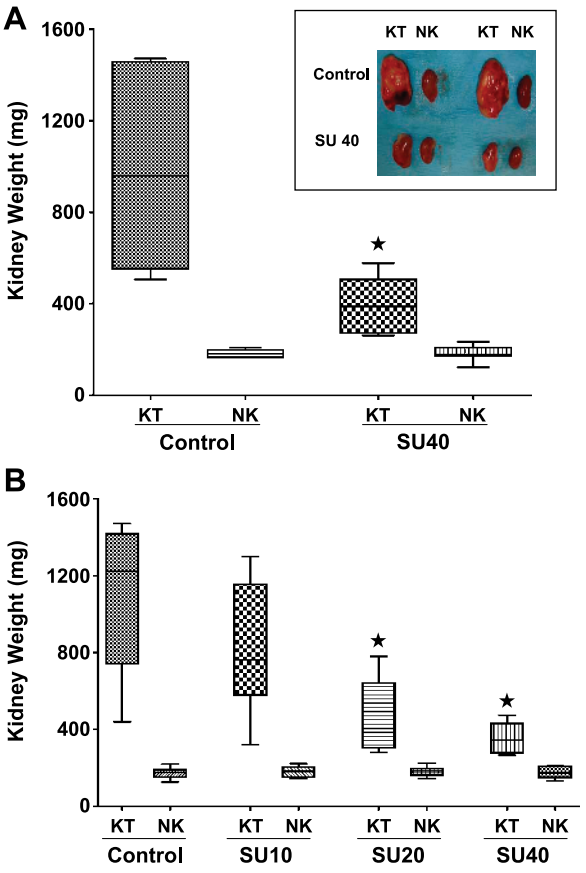

Figure 4. KCI-18 KT response to sunitinib. Mice bearing established KTs were treated daily with sunitinib for 18 days, then tumors were resected and weighted. (A) Response to optimal dose of sunitinib. The kidney weights and their median are reported for 10 mice per group treated with vehicle (control) or sunitinib at 40 mg/kg per day (SU40) compared with the contralateral NK weights in each experimental group. Inset contains pictures of KTs of control mice or SU40-treated mice compared with NKs. (B) Sunitinib dose-response. The kidney weights and their median are reported for eight mice per group treated with vehicle (control) or sunitinib at dosages of 40, 20, or 10 mg/kg per day (SU40, SU20, or SU10, respectively) compared with the contralateral NK weights in each experimental group. *P < .05. Data presented were obtained from separate representative experiments.

Effect of Sunitinib on the Vasculature of KTs

For histologic studies, KT sections were stained with H&E or by immunostaining with anti-CD31 Ab for the detection of blood vessels. KTs presented as high-grade carcinomas, consisting of tumor cells with large pleomorphic nuclei, prominent nucleoli, abundant eosinophilic cytoplasm, and large cytoplasmic inclusions (Figure 5*A*, *Control*) [34]. These tumors were highly vascularized with a sinusoidal vascular pattern and abnormal enlarged vessels as seen both by H&E staining and anti-CD31 staining (Figure 5, *A* and *B*, *Control*). Tumors treated with SU40 showed areas of tumor destruction and necrosis associated with hemorrhages but also remaining areas of viable tumor cells (Figure 5*A*). The destruction of tumor vasculature was confirmed by anti-CD31 staining with disruption of the vessel walls, release of red blood cells in the tumor, and minimal staining of endothelial cells by anti-CD31 (Figure 5*B*). KTs treated with SU20 clearly showed more regularized and thinner vessels by H&E, and staining of endothelial cells in the vessel walls by anti-CD31 (Figure 5, *A* and *B*) in contrast to the enlarged abnormal vessels observed in KTs from control mice. However, tumors treated with SU10 still contained enlarged abnormal vessels as confirmed by anti-CD31 staining (Figure 5, *A* and *B*), and some of them were comparable to those observed in control mice.

Effect of Sunitinib on Vasculature of NK Tissue

Histologic analysis of NKs obtained from control mice showed multiple regular and thin vessels by H&E (Figure 6*A*) and clear structures of vessels delineated by anti-CD31 staining of endothelial cells in vessel walls (Figure 6*B*). In contrast, NKs obtained from mice treated with the high SU40 dosage showed dilatation of blood vessels as seen by H&E (Figure 6*A*). Some enlarged vessels showed disruption of vessel walls as observed by anti-CD31 staining (Figure 6*B*). The effect of SU20 on normal vessels in NKs was mild and caused dilatation only in a few vessels, whereas most looked normal as seen by anti-CD31 staining, in contrast to the numerous vessels enlarged by SU40 treatment (Figure 6, *A* and *B*). No effect on vessels in the NK was observed

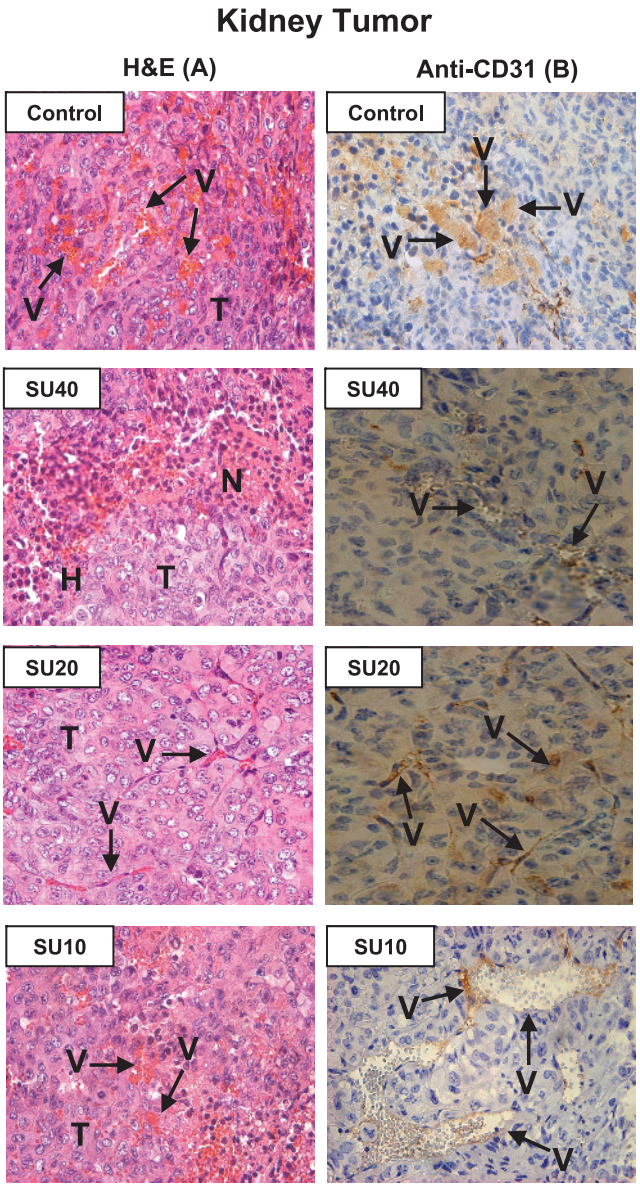

Figure 5. Histologic diagnosis of KCI-18 KTs treated with various dosages of sunitinib. KTs resected from mice for the experiments described in Figure 4 were processed for histologic diagnosis, and tumor sections were stained either with H&E (A) or with anti-CD31 immunostaining (B). *H* indicates hemorrhages; *N*, necrosis; *T*, tumor; *V*, vessels. Control untreated tumors consisted of tumor cells with large pleomorphic nuclei and were highly vascularized with a sinusoidal vascular pattern and abnormal enlarged vessels. Tumors treated with SU40 showed areas of tumor destruction and necrosis associated with hemorrhages and areas of viable tumor cells. Tumor sections stained with anti-CD31 reveal destruction of tumor vasculature and disruption of the vessel walls. KTs treated with SU20 showed more regularized and thinner vessels both by H&E and by anti-CD31 staining. SU10-treated tumors show enlarged abnormal vessels as confirmed by anti-CD31 staining with staining of areas of endothelial cells lining vessel walls. Original magnifications, ×40.

with SU10; the vessels looked thin and regular and were comparable to those seen in NKs of control mice (Figure 6, *A* and *B*). It should be noted that although disruptions in normal vessels were observed after sunitinib therapy, the mice treated with dosages of 20 to 40 mg/kg per day showed no apparent signs of drug toxicity.

Direct Cytotoxic Effect of Sunitinib and Expression of VEGFR-2 and PDGFR-β on KCI-18 Cells and KTs

To determine whether sunitinib has a direct cytotoxic effect on KCI-18 RCC, cells were treated *in vitro* with various doses and plated in colony formation assay [37]. Compared with control cells treated with vehicle, a significant dose-dependent effect was observed at doses

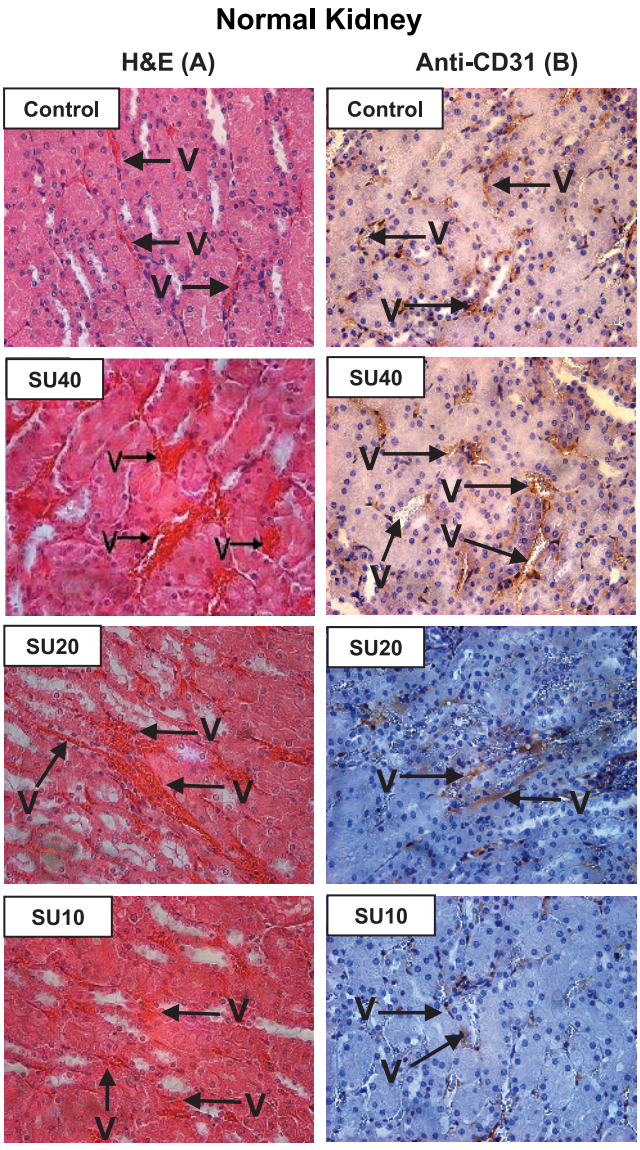

Figure 6. Histologic diagnosis of NKs from mice treated with various doses of sunitinib. The contralateral left NKs (not bearing a tumor) resected from mice of the experiments described in Figure 4 were processed for histologic diagnosis, and kidney tissue sections were stained either with H&E (A) or with anti-CD31 immunostaining (B). NKs obtained from control mice showed multiple regular and thin vessels (V) by H&E and clear structures of vessels delineated by anti-CD31 staining of endothelial cells in vessel walls. After high SU40 dosage, dilatation of blood vessels was observed as seen by H&E. Enlarged vessels sometimes showed disruption of vessel walls seen by anti-CD31 staining. The milder effect of SU20 on normal vessels in NKs caused dilatation only in a few vessels, whereas most looked normal as seen by anti-CD31 staining. No effect on vessels in the NK was observed with SU10; the vessels looked thin and regular. Original magnifications, ×40.

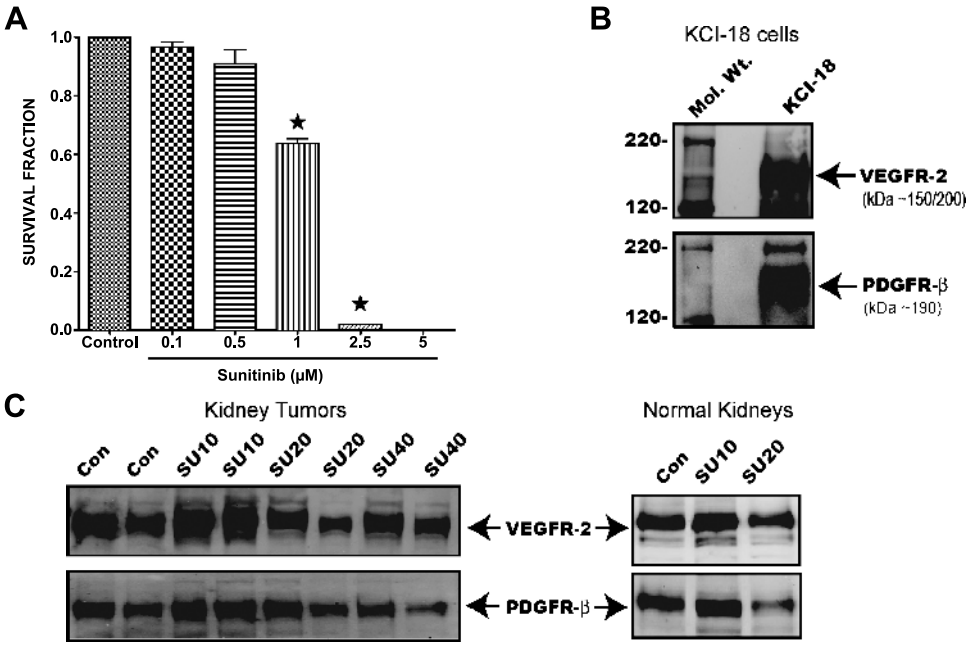

Figure 7. Survival fraction of KCl-18 cells treated with sunitinib and expression of VEGFR-2 and PDGFR-β sunitinib targets on cells and tumors. (A) Inhibition of cell growth *in vitro*. KCl-18 cells were treated with sunitinib doses of 0.1 to 5 μM and plated in a colony formation assay for 10 days. Bars represent the mean survival fraction ± SEM of triplicate wells. (B and C) Expression of VEGFR-2 and PDGFR-β on KCl-18 cells and tumors. KCl-18 cells or KTs were lysed, and protein extracts were first immunoprecipitated with anti–VEGFR-2 or anti–PDGFR-β Abs. Immune complexes were separated using protein A agarose beads, and the expression of VEGFR-2 and PDGFR-β was determined by Western blot analysis. (B) Expression of VEGFR-2 or anti–PDGFR-β on KCl-18 cells. (C) Expression of VEGFR-2 or PDGFR-β in KCl-18 KTs and NKs from mice treated with SU10, SU20, or SU40 compared with control (Con) mice.

greater than 0.5 μM with 40% inhibition in survival at 1 μM and complete cell killing at 2.5 to 5 μM ($P < .05$; Figure 7*A*).

The effect of sunitinib on expression of RTKs targets, VEGFR-2 and PDGFR-β, was determined by Western blot analysis of cultured cells and KTs. Both VEGFR-2 and PDGFR-β receptors showed a high expression on KCI-18 cells cultured *in vitro* (Figure 7*B*), confirming that our KCI-18 RCC cell line expresses these receptors. KTs obtained from mice treated with various doses of sunitinib for 7 days *in vivo* were also tested for expression of RTKs. Both VEGFR-2 and PDGFR-β receptors were strongly expressed by KCI-18 KTs in control mice (Figure 7*C*). A trend to increased expression of VEGFR-2 and PDGFR-β was observed after treatment with a low dosage of SU10 (Figure 7*C*). At higher dosages of SU20 and SU40, a trend to decreased expression of VEGFR-2 and PDGFR-β receptors was observed (Figure 7*C*). Interestingly, modulation of VEGFR-2 and PDGFR-β receptors was also observed in NKs, with increased expression in SU10-treated mice and lower expression in SU20-treated mice (Figure 7*C*).

Discussion

To design novel targeted therapies for metastatic RCC, extensive research is ongoing to test drugs that target both the tumor cells and the tumor vasculature to inhibit processes that stimulate tumor growth in the tumor microenvironment. Antiangiogenic therapy causing excessive vascular regression could compromise the delivery of drugs or oxygen in the tumor when combined with conventional cytotoxic therapies [21,22]. Using a preclinical RCC model, we have investigated, by DCE-MRI, vascular changes in KTs induced by the antiangiogenic drug sunitinib to select doses that could induce transient vessel normalization by pruning inefficient blood vessels and thereby improve tumor blood flow and subsequent drug delivery to tumor cells by chemotherapy [25–27,39].

A dose-dependent therapeutic efficacy of sunitinib for KCI-18 RCC tumor xenografts was demonstrated with dosages of 20 and 40 mg/kg per day, causing a significant inhibition/arrest of tumor growth and limited invasion of the kidney by tumor cells, in agreement with previous preclinical animal studies [7–13]. Sunitinib exerted a direct cytotoxic effect at doses greater than 0.5 μM in KCI-18 cells *in vitro*. As documented in clear cell RCC and papillary RCC human tumor specimens [13,40], we found that KCI-18 cells and tumors also expressed the VEGFR-2 and PDGFR-β RTKs targets of sunitinib. Increasing doses of sunitinib caused a lower expression of these receptors on KTs, probably due to the modulation of these receptors. These findings suggest that sunitinib could inhibit KCI-18 tumor growth through targeting of RTKs signaling on tumor cells and/or on endothelial cells or stromal cells resulting in direct antitumor and antiangiogenic activities as shown in other studies [7]. Interestingly, modulation of RTKs receptors by sunitinib was also observed on NK tissues, confirming the effect of the drug on the vasculature of normal tissues. In agreement with our findings, recent animal studies [41] and clinical trials of sunitinib for metastatic RCC or breast cancer reported decreased soluble VEGFRs' plasma levels [42,43], which suggested modulation of VEGF pathway biomarkers by sunitinib. Furthermore, previous pharmacokinetic studies in mouse xenograft models demonstrated plasma levels of 50 to 100 ng/ml for 12 hours when mice were treated with the same efficacious dosages of 20 to 40 mg/kg per day of sunitinib as used in our studies, resulting in the inhibition of VEGFR-2 and PDGFR-β RTKs [7]. Comparable plasma levels of 50 to 100 ng/ml of sunitinib were also measured in pharmacokinetic studies of patients receiving 50-mg daily doses [44].

Sunitinib also induced dose-dependent vascular changes, which were observed both in KTs and in NK tissues by DCE-MRI. In control mice, the clearance of Gd in the KT was slow compared with faster clearance in the NK, probably as a result of leakiness from the abnormal enlarged tumor vessels observed histologically. Parametric maps from control mice showed accumulation of Gd in the periphery of the tumor with no uptake in the core of the tumor, indicative of poor vascularity and perfusion in the core of the tumor as shown in other MRI studies of xenograft tumors [32,33]. In contrast, the NK of control mice showed distribution of Gd in the entire kidney with lower uptake in the peripheral cortex and a higher uptake in the medulla probably due to greater numbers of vessels in that area and reflecting normal secretion of contrast agent. Compared with control tumors, KTs from mice treated with a low dosage of 10 mg/kg per day of sunitinib showed mild changes in Gd uptake and clearance kinetics of KTs. These SU10-treated tumors had also poor tumor perfusion in the core of the tumor and histologically showed enlarged abnormal vessels similar to findings observed in control tumors. Likewise, SU10 caused minimal effect on NK tissue vasculature with no changes in vascular permeability or vessel morphology compared with control mice.

A therapeutic high dosage of 40 mg/kg per day induced vascular permeability changes resulting in retention of Gd in both left and right kidneys. Gd retention was greater in the KT than in the NK. This increased vascular permeability of Gd in the tumor could be due to the damaged vasculature and leakage of Gd into surrounding kidney tissue with slow kinetics of washout. Histologic studies confirmed destruction of tumor vasculature of SU40-treated KTs and disruption of the vessel walls causing hemorrhages. It should be noted that increased levels of Gd were also observed in both cortex and medulla of NKs, indicating that this high SU40 dosage alters the kinetics of uptake and contrast clearance of NK tissue. These data are supported by histologic observation of dilatation and disruption of normal vessels detected by anti-CD31 Ab staining of NK tissue. We conclude that the dosage of 40 mg/kg per day of sunitinib causes excessive vascular damage and vascular permeability in KTs and alterations of NK vessels. This in turn suggests that this dosage is not appropriate for combination chemotherapies.

After treatment with an intermediate sunitinib dosage of 20 mg/kg per day, improved Gd clearance was observed with less Gd retention than that seen with SU40 or in control mice. Interestingly, in SU20-treated mice, Gd uptake and clearance in the $C(t)$ curves, IAUC, and CIAUC showed identical patterns in the KT compared with the NK as confirmed by the low R50 value of KTs relative to the R50 value of NKs (Figure 2*D*). A clear shift to the left of IAUC curves of SU20-treated mice was observed compared with control mice and SU40-treated mice as shown also by the low R50 value of KTs treated with SU20 relative to the R50 value of control KTs (Figure 2*E*). These data suggest a return to more "normal vasculature" with lower permeability (i.e., less leaky vessels) after treatment with SU20. Interestingly, a similar pattern was observed in NKs of mice treated with sunitinib compared with those of control mice showing NR50 values lower for SU20-treated mice than for SU40-treated mice, indicating a milder effect of SU20 dosage on vasculature of NK tissue (Figure 2*F*). Parametric maps revealed increased Gd uptake in the core of the tumor and surrounding kidney tissue in SU20-treated mice. Histologically, the vessels of KTs treated with SU20 clearly showed more regularized and thinner vessels, indicating pruning or normalization of tumor vessels compared with the enlarged vessels of control KTs. The effect of SU20 on vessels in NKs was mild and caused dilatation only in a few vessels.

In summary, imaging of tumor vasculature changes by DCE-MRI and histologic diagnosis indicates that a lower dosage of 20 mg/kg per day of sunitinib could cause "pruning" or normalization of the tumor vasculature allowing for better tumor perfusion and decreased leakiness of vessels. Moreover, this dosage caused only mild vascular changes in normal tissues and thus could be less toxic to normal vessels, suggesting that this dosage could be used for combination with chemotherapy or radiotherapy.

Our histologically verified studies demonstrate that the use of DCE-MRI is a useful means for monitoring vascular changes induced by sunitinib in both tumors and normal tissues. These data can be used to select the dose and schedule of sunitinib and potentially other anti-angiogenic drugs causing transient normalization of tumor vasculature for combination therapies.

Acknowledgments

The authors thank Yimin Shen for excellent technical assistance with DCE-MRI and Bijoyananda Adhikary for help with data analysis. The authors thank Maria Vlachaki and Ulka Vaishampayan (Karmanos Cancer Institute) for stimulating discussions on clinical translation issues.

References

[1] Jemal A, Siegel R, Ward E, Hao Y, Xu J, Murray T, and Thun MJ (2008). Cancer statistics, 2008. *CA Cancer J Clin* **58**, 71–96.

[2] Haas GP and Hillman GG (1996). Update on the role of immunotherapy in the management of kidney cancer. *Cancer Control* **3**, 536–541.

[3] Motzer RJ, Bander NH, and Nanus DM (1996). Renal-cell carcinoma. *N Engl J Med* **335**, 865–875.

[4] Flanigan RC, Salmon SE, Blumenstein BA, Bearman SI, Roy V, McGrath PC, Caton JR Jr, Munshi N, and Crawford ED (2001). Nephrectomy followed by interferon α-2b compared with interferon α-2b alone for metastatic renal-cell cancer. *N Engl J Med* **345**, 1655–1659.

[5] Folkman J (2006). Angiogenesis. *Annu Rev Med* **57**, 1–18.

[6] Kerbel R and Folkman J (2002). Clinical translation of angiogenesis inhibitors. *Nat Rev Cancer* **2**, 727–739.

[7] Mendel DB, Laird AD, Xin X, Louie SG, Christensen JG, Li G, Schreck RE, Abrams TJ, Ngai TJ, Lee LB, et al. (2003). *In vivo* antitumor activity of SU11248, a novel tyrosine kinase inhibitor targeting vascular endothelial growth factor and platelet-derived growth factor receptors: determination of a pharmacokinetic/pharmacodynamic relationship. *Clin Cancer Res* **9**, 327–337.

[8] Abrams TJ, Lee LB, Murray LJ, Pryer NK, and Cherrington JM (2003). SU11248 inhibits KIT and platelet-derived growth factor receptor β in preclinical models of human small cell lung cancer. *Mol Cancer Ther* **2**, 471–478.

[9] Abrams TJ, Murray LJ, Pesenti E, Holway VW, Colombo T, Lee LB, Cherrington JM, and Pryer NK (2003). Preclinical evaluation of the tyrosine kinase inhibitor SU11248 as a single agent and in combination with "standard of care" therapeutic agents for the treatment of breast cancer. *Mol Cancer Ther* **2**, 1011–1021.

[10] Murray LJ, Abrams TJ, Long KR, Ngai TJ, Olson LM, Hong W, Keast PK, Brassard JA, O'Farrell AM, Cherrington JM, et al. (2003). SU11248 inhibits tumor growth and CSF-1R–dependent osteolysis in an experimental breast cancer bone metastasis model. *Clin Exp Metastasis* **20**, 757–766.

[11] O'Farrell AM, Abrams TJ, Yuen HA, Ngai TJ, Louie SG, Yee KW, Wong LM, Hong W, Lee LB, Town A, et al. (2003). SU11248 is a novel FLT3 tyrosine kinase inhibitor with potent activity *in vitro* and *in vivo*. *Blood* **101**, 3597–3605.

[12] Sohal J, Phan VT, Chan PV, Davis EM, Patel B, Kelly LM, Abrams TJ, O'Farrell AM, Gilliland DG, Le Beau MM, et al. (2003). A model of APL with FLT3 mutation is responsive to retinoic acid and a receptor tyrosine kinase inhibitor, SU11657. *Blood* **101**, 3188–3197.

[13] Xu L, Tong R, Cochran DM, and Jain RK (2005). Blocking platelet-derived growth factor-D/platelet-derived growth factor receptor β signaling inhibits human renal cell carcinoma progression in an orthotopic mouse model. *Cancer Res* **65**, 5711–5719.

[14] Motzer RJ, Michaelson MD, Redman BG, Hudes GR, Wilding G, Figlin RA, Ginsberg MS, Kim ST, Baum CM, DePrimo SE, et al. (2006). Activity of

SU11248, a multitargeted inhibitor of vascular endothelial growth factor receptor and platelet-derived growth factor receptor, in patients with metastatic renal cell carcinoma. *J Clin Oncol* **24**, 16–24.

[15] Motzer RJ, Hutson TE, Tomczak P, Michaelson MD, Bukowski RM, Rixe O, Oudard S, Negrier S, Szczylik C, Kim ST, et al. (2007). Sunitinib versus interferon α in metastatic renal-cell carcinoma. *N Engl J Med* **356**, 115–124.

[16] Motzer RJ, Hutson TE, Tomczak P, Michaelson MD, Bukowski RM, Oudard S, Negrier S, Szczylik C, Pili R, Bjarnason GA, et al. (2009). Overall survival and updated results for sunitinib compared with interferon alfa in patients with metastatic renal cell carcinoma. *J Clin Oncol*, 2009 June 1. [Epub ahead of print].

[17] Kollmannsberger C, Soulieres D, Wong R, Scalera A, Gaspo R, and Bjarnason G (2007). Sunitinib therapy for metastatic renal cell carcinoma: recommendations for management of side effects. *Can Urol Assoc J* **1**, S41–S54.

[18] Chu TF, Rupnick MA, Kerkela R, Dallabrida SM, Zurakowski D, Nguyen L, Woulfe K, Pravda E, Cassiola F, Desai J, et al. (2007). Cardiotoxicity associated with tyrosine kinase inhibitor sunitinib. *Lancet* **370**, 2011–2019.

[19] Telli ML, Witteles RM, Fisher GA, and Srinivas S (2008). Cardiotoxicity associated with the cancer therapeutic agent sunitinib malate. *Ann Oncol* **19**, 1613–1618.

[20] Schmidinger M, Zielinski CC, Vogl UM, Bojic A, Bojic M, Schukro C, Ruhsam M, Hejna M, and Schmidinger H (2008). Cardiac toxicity of sunitinib and sorafenib in patients with metastatic renal cell carcinoma. *J Clin Oncol* **26**, 5204–5212.

[21] Jain RK (2005). Normalization of tumor vasculature: an emerging concept in antiangiogenic therapy. *Science* **307**, 58–62.

[22] Jain RK (2001). Normalizing tumor vasculature with anti-angiogenic therapy: a new paradigm for combination therapy. *Nat Med* **7**, 987–989.

[23] Winkler F, Kozin SV, Tong RT, Chae SS, Booth MF, Garkavtsev I, Xu L, Hicklin DJ, Fukumura D, di Tomaso E, et al. (2004). Kinetics of vascular normalization by VEGFR2 blockade governs brain tumor response to radiation: role of oxygenation, angiopoietin-1, and matrix metalloproteinases. *Cancer Cell* **6**, 553–563.

[24] Lee CG, Heijn M, di Tomaso E, Griffon-Etienne G, Ancukiewicz M, Koike C, Park KR, Ferrara N, Jain RK, Suit HD, et al. (2000). Anti–vascular endothelial growth factor treatment augments tumor radiation response under normoxic or hypoxic conditions. *Cancer Res* **60**, 5565–5570.

[25] Browder T, Butterfield CE, Kraling BM, Shi B, Marshall B, O'Reilly MS, and Folkman J (2000). Antiangiogenic scheduling of chemotherapy improves efficacy against experimental drug–resistant cancer. *Cancer Res* **60**, 1878–1886.

[26] Klement G, Baruchel S, Rak J, Man S, Clark K, Hicklin DJ, Bohlen P, and Kerbel RS (2000). Continuous low-dose therapy with vinblastine and VEGF receptor-2 antibody induces sustained tumor regression without overt toxicity. *J Clin Invest* **105**, R15–R24.

[27] Wildiers H, Guetens G, De Boeck G, Verbeken E, Landuyt B, Landuyt W, de Bruijn EA, and van Oosterom AT (2003). Effect of antivascular endothelial growth factor treatment on the intratumoral uptake of CPT-11. *Br J Cancer* **88**, 1979–1986.

[28] Yankeelov TE, Lepage M, Chakravarthy A, Broome EE, Niermann KJ, Kelley MC, Meszoely I, Mayer IA, Herman CR, McManus K, et al. (2007). Integration of quantitative DCE-MRI and ADC mapping to monitor treatment response in human breast cancer: initial results. *Magn Reson Imaging* **25**, 1–13.

[29] Jackson A, O'Connor JP, Parker GJ, and Jayson GC (2007). Imaging tumor vascular heterogeneity and angiogenesis using dynamic contrast-enhanced magnetic resonance imaging. *Clin Cancer Res* **13**, 3449–3459.

[30] Hahn OM, Yang C, Medved M, Karczmar G, Kistner E, Karrison T, Manchen E, Mitchell M, Ratain MJ, and Stadler WM (2008). Dynamic contrast-enhanced magnetic resonance imaging pharmacodynamic biomarker study of sorafenib in metastatic renal carcinoma. *J Clin Oncol* **26**, 4572–4578.

[31] Hylton N (2006). Dynamic contrast-enhanced magnetic resonance imaging as an imaging biomarker. *J Clin Oncol* **24**, 3293–3298.

[32] Checkley D, Tessier JJ, Kendrew J, Waterton JC, and Wedge SR (2003). Use of dynamic contrast-enhanced MRI to evaluate acute treatment with ZD6474, a VEGF signalling inhibitor, in PC-3 prostate tumours. *Br J Cancer* **89**, 1889–1895.

[33] Marzola P, Degrassi A, Calderan L, Farace P, Nicolato E, Crescimanno C, Sandri M, Giusti A, Pesenti E, Terron A, et al. (2005). Early antiangiogenic activity of SU11248 evaluated *in vivo* by dynamic contrast-enhanced magnetic resonance imaging in an experimental model of colon carcinoma. *Clin Cancer Res* **11**, 5827–5832.

[34] Gaustad JV, Brurberg KG, Simonsen TG, Mollatt CS, and Rofstad EK (2008). Tumor vascularity assessed by magnetic resonance imaging and intravital microscopy imaging. *Neoplasia* **10**, 354–362.

[35] Hillman GG, Wang Y, Che M, Raffoul JJ, Yudelev M, Kucuk O, and Sarkar FH (2007). Progression of renal cell carcinoma is inhibited by genistein and radiation in an orthotopic model. *BMC Cancer* **7**, 4.

[36] Haacke EM, Filleti CL, Gattu R, Ciulla C, Al-Bashir A, Suryanarayanan K, Li M, Latif Z, DelProposto Z, Sehgal V, et al. (2007). New algorithm for quantifying vascular changes in dynamic contrast-enhanced MRI independent of absolute T1 values. *Magn Reson Med* **58**, 463–472.

[37] Raffoul JJ, Banerjee S, Singh-Gupta V, Knoll ZE, Fite A, Zhang H, Abrams J, Sarkar FH, and Hillman GG (2007). Down-regulation of apurinic/apyrimidinic endonuclease 1/redox factor-1 expression by soy isoflavones enhances prostate cancer radiotherapy *in vitro* and *in vivo*. *Cancer Res* **67**, 2141–2149.

[38] Holm S (2009). A simple sequentially rejective multiple test procedure. *Scand J Statist* **6**, 65–70.

[39] Tong RT, Boucher Y, Kozin SV, Winkler F, Hicklin DJ, and Jain RK (2004). Vascular normalization by vascular endothelial growth factor receptor 2 blockade induces a pressure gradient across the vasculature and improves drug penetration in tumors. *Cancer Res* **64**, 3731–3736.

[40] Lam JS, Leppert JT, Figlin RA, and Belldegrun AS (2005). Role of molecular markers in the diagnosis and therapy of renal cell carcinoma. *Urology* **66**, 1–9.

[41] Ebos JM, Lee CR, Christensen JG, Mutsaers AJ, and Kerbel RS (2007). Multiple circulating proangiogenic factors induced by sunitinib malate are tumor-independent and correlate with antitumor efficacy. *Proc Natl Acad Sci USA* **104**, 17069–17074.

[42] Burstein HJ, Elias AD, Rugo HS, Cobleigh MA, Wolff AC, Eisenberg PD, Lehman M, Adams BJ, Bello CL, DePrimo SE, et al. (2008). Phase II study of sunitinib malate, an oral multitargeted tyrosine kinase inhibitor, in patients with metastatic breast cancer previously treated with an anthracycline and a taxane. *J Clin Oncol* **26**, 1810–1816.

[43] Rini BI, Michaelson MD, Rosenberg JE, Bukowski RM, Sosman JA, Stadler WM, Hutson TE, Margolin K, Harmon CS, DePrimo SE, et al. (2008). Antitumor activity and biomarker analysis of sunitinib in patients with bevacizumab-refractory metastatic renal cell carcinoma. *J Clin Oncol* **26**, 3743–3748.

[44] Britten CD, Kabbinavar F, Hecht JR, Bello CL, Li J, Baum C, and Slamon D (2008). A phase I and pharmacokinetic study of sunitinib administered daily for 2 weeks, followed by a 1-week off period. *Cancer Chemother Pharmacol* **61**, 515–524.